Non-disruptive MHD Dynamics in Inward-shifted LHD Configurations

H. Miura 1), K. Ichiguchi 1), N. Nakajima 1), T. Hayashi 1) and B.A. Carreras 2)

1)National Institute for Fusion Science, 322-6 Oroshi, Toki, Gifu 509-5292, JAPAN
2)Oak Ridge National Laboratory, Oak Ridge, Tennessee 37831, USA

e-mail contact of main author:miura.hideaki@nifs.ac.jp

Abstract. Two kinds of nonlinear simulations are conducted to study behaviors of the pressure-driven modes in the Large Helical Device (LHD) plasma with the vacuum magnetic axis located at $R_{ax} = 3.6$m (so called inward-shifted configuration). One is the three-field reduced magnetohydrodynamic (RMHD) simulations. The other is the direct numerical simulations (DNS) of fully three-dimensional (3D) compressible MHD equations. The RMHD results suggest that the plasma behavior depends on the strength of the interaction between the unstable modes with different helicity. Similar plasma behaviors are also obtained in the DNS. In addition to some basic coincidence between RMHD and DNS, substantial toroidal flow generation is observed in the DNS. It is shown that toroidal flow can become stronger than the poloidal flow.

1 Introduction

The Large Helical Device (LHD) is a heliotron type device with a set of L=2/M=10 helical coils with the major radius 3.9m [1]. When the position of the vacuum magnetic axis R_{ax} is smaller than 3.75m, the system is called “inward-shifted” configuration. Recent advances of the LHD experiments in inward-shifted configurations show that plasma is confined relatively well even though it passes through Mercier unstable region [2, 3]. It is reported in Refs.[2, 3] with $R_{ax} = 3.6m$ vacuum magnetic axis, MHD instabilities with poloidal(m) and toroidal(n) Fourier modes $(m,n) = (2,1)$ appears in the course of the plasma pressure growth but disappears when the pressure (or the β value, $\beta = 2p/|\mathbf{B}|^2$ where p is the pressure and $\mathbf{B}$ represents the magnetic field vector) becomes sufficiently large. In stead of $(2,1)$, $(1,1)$ and $(2,3)$ modes whose resonant surfaces are in the neighbourhood of the outermost magnetic surfaces appear to dominate the fluctuations. Although these MHD instability are observed, the plasma confinement are maintained longer than we expect from its unstable properties of the configuration. It is now required to clarify the reason of the good confinement because it can bring about good confinement in further high-β state.

An explanation for the good confinement in the linearly unstable region was proposed by Ichiguchi et al. based on the three-field RMHD simulations[4]. They found that strong overlap of the vortices with different helicity causes a disruptive phenomenon. They showed that such disruptive phenomenon can be suppressed by the self-organized deformation of the pressure profile which results from the nonlinear evolution of the interchange mode itself at lower β value. In the present study, this stabilization scenario is further confirmed for higher β value than those in the previous work.

Though the RMHD simulations have tractable natures to investigate the complex helical-toroidal system, the approximation used to derive the RMHD equations restrict their applicability. For example, the compressibility and poloidal motions are assumed to be negligible in the three-field RMHD equations. It is desirable to investigate effects of physical mechanism which are not incorporated in the RMHD system to study plasma dynamics more precisely and reach to a conclusive understanding. Here the direct numerical simulation (DNS) code of the 3D compressible and nonlinear MHD equations developed by Miura et al[5] are made use of for this purpose. The code includes most of essences of MHD dynamics such as compressibility and toroidal flows. Hereafter we call these which are included in the DNS and not included in RMHD as "full MHD effects". We examine how the full MHD effects appear in the plasma evolution in LHD from the view points of detailed MHD dynamics.

2 RMHD simulations

The RMHD simulations are conducted by the use of the NORM code. The toroidal geometry is incorporated by utilizing the toroidally averaged equilibrium quantities, which is obtained by using the 3D equilibrium calculated with the VMEC code[6]. Details of the code are given in Ref.[4]. In order to consider the stabilizing mechanism for the interchange mode in the LHD plasma, we have focused on the evolution of the pressure profile in the increase of the β value. In the present RMHD simulations, the magnetic Reynolds number is assumed to be $S = 10^6$ and the fixed boundary condition is employed.

We start from the investigation of the interchange mode at $\beta_0 = 0.5\%$, where β_0 denotes the β value at the magnetic axis. The initial equilibrium is calculated with the almost parabolic pressure profile of $p_{eq} = p_0(1-\rho^2)(1-\rho^8)$ under the constraints of the no net current, where ρ is the square-root of the normalized toroidal flux. This pressure profile is consistent with the experimental data at low β.[7] This equilibrium is unstable against the linear ideal interchange mode. In the time evolution, the $(m,n) = (5,2)$, $(7,3)$ and $(2,1)$ modes are excited. However, all of them are saturated mildly without disruptive behavior. This is due to the fact that the vortices of the modes are localized around the corresponding rational surfaces, and therefore, they do not overlap each other. Such mild saturation results in the generation of the local flat regions in the average component of pressure profile $\langle p \rangle$, as shown by the blue line in FIG.1. Here $\langle p \rangle$ is defined as $\langle p \rangle = \oint\oint p d\theta d\zeta$, where θ and ζ denote the poloidal and toroidal angles, respectively.

Next we consider the increase of the β value to $\beta_0 = 1.0\%$. In the nonlinear calculation with the initial pressure profile fixed to the parabolic one, a disruptive phenomenon is obtained[4]. In this case, the pressure in the central region is decreased in a short time. This phenomenon is caused by the significant overlap of the vortices due to the enhancement of the driving force. On the other hand, the actual pressure profile changes continuously in the increase of the β value. In order to simulate this situation, we employ the profile of the saturated pressure in the calculation at $\beta_0 = 0.5\%$ as the initial pressure profile of the nonlinear calculation at $\beta_0 = 1.0\%$. In this case, the interaction of the vortices is weak and the unstable modes are mildly saturated as in the case of $\beta_0 = 0.5\%$. The disruptive phenomenon is suppressed because the locally flat structure in the initial pressure profile reduces the driving force at the resonant surfaces. The saturated average pressure profile is shown by the purple line in FIG.1.

In order to examine whether this mechanism explains the stable LHD plasma at higher β value, we investigate the nonlinear behavior at $\beta_0 = 1.5\%$ by applying this scheme. The saturated pressure profile at $\beta_0 = 1.0\%$ is employed as the initial profile. In the nonlinear evolution, the fluctuations are saturated mildly and the resultant pressure profile also shows the locally flat structure again. (See the red solid line in FIG.1.) Figure 2 shows the bird's eye view of this pressure profile at $\beta_0 = 1.5\%$. The profile is not only locally flattened in the average component but also reorganized to have a precise structures corresponding to the poloidal mode number of the saturated mode at each resonant surface. This structure is formed by the local vortices of the interchange mode. This result shows that the disruptive phenomenon is suppressed by the local deformation of the pressure profile in the series of the β value. Thus, it still suggests that the the self-organization of the pressure profile due to the interchange mode can be the main stabilizing mechanism in the LHD plasma.

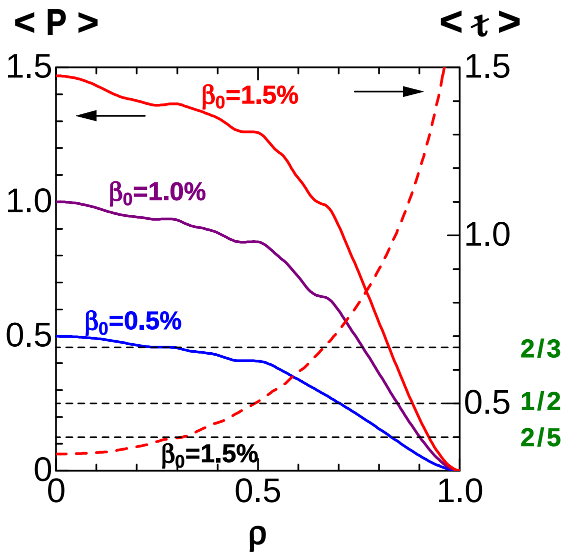

FIG. 1: Average pressure profile in the non-linear saturated stage in the series of the β value.

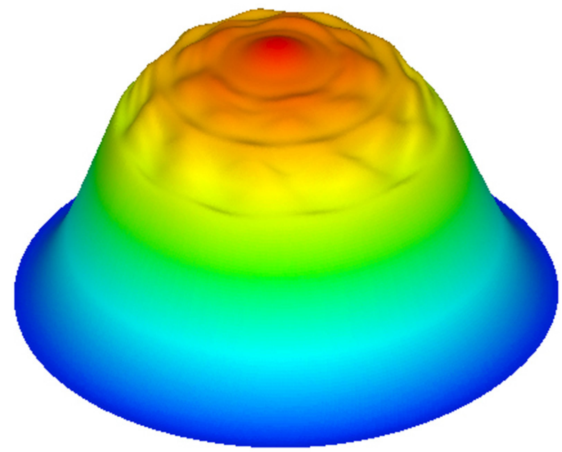

FIG. 2: Bird's-eye view of pressure profile at $\beta_0 = 1.5\%$.

3 DNS of full 3D compressible MHD

3.1 Unstable Fourier mode growth

Here DNS of the 3D compressible and nonlinear MHD equations is conducted. We pay special attention to detailed MHD dynamics which are brought about by the full MHD effects. In the analysis we make use of the Boozer coordinate system *for the initial equilibrium*. The Boozer coordinates (ρ, θ, ζ) is obtained by the use of the HINT[8] and VMEC[6].

There are some numerical results which have been obtained earlier by the DNS code. The first work[5] is on simulations under the L=2/M=10 stellarator symmetry of the LHD, in which $(m,n) \simeq (15,10)$ and $(20,10)$ resistive ballooning modes are excited sequentially and saturated mildly. Next, full-torus DNS has been carried out[10, 11]. In the full-torus simulations, DNS under the stellarator symmetry are carried out prior to them so as to skip the long quasi-stationary period. (Hereafter we call the DNS under the stellarator symmetry prior to the full-torus simulation simply as the pre-calculation.) In FIG.3, the averaged pressure profile $\langle p \rangle$ is shown as the function of ρ. The red solid line is the ideal MHD equilibrium with $R_{ax} = 3.6m$ and $\beta_0 = 4\%$ provided by the HINT code[8]. The green line represents $\langle p \rangle$ of the initial condition for the full-torus simulation[10, 11] provided by the pre-calculation. It is seen in FIG.3 that the pressure gradient becomes less steep by the pre-calculation. In the full-torus simulation starting from the less-steep pressure gradient, the pressure-driven instability leads to formation of two pairs of mushroom-like structures of the pressure associated with the $(m,n) = (2,1)$ mode[10]. The structure formation is similar to those observed in RMHD simulations. Furthermore, we have found that toroidal flow grows as energetic as poloidal flows in the simulation[11]. In these earlier DNS, the pressure-driven modes are saturated mildly whether the system is under the stellarator symmetry or full-torus.

Since the plasma behaviors are sensitive to the initial pressure profile, the pre-calculations may have brought about qualitative changes to the plasma behaviors. It is worth carrying out the full-torus DNS starting from the HINT equilibrium, without the pre-calculation, and studying detailed physical process in it in order to find out what classifies the plasma behaviors disruptive or non-disruptive. For simplicity, we call the full-torus simulation starting from the pre-calculated initial condition as "run 1" and the one starting from the HINT equilibrium as "run 2". The magnetic Reynolds number is set $S = 10^6$ in both runs. Figure 4 shows time evolutions of the kinetic energy $K = \left\langle \rho_m \mathbf{v}^2 \right\rangle /2$ and the poloidal contribution to it $K_P = \left\langle \rho_m \mathbf{v}_P^2 \right\rangle /2$ in runs 1 and 2, where ρ_m, $\mathbf{v}$ and $\mathbf{v}_P$ are the mass density, the total velocity vector, poloidal part of the velocity, respectively. At early stages in the two runs, main parts of the kinetic energy K come from K_P. When $K \simeq K_P$, the fluid motions are nearly two-dimensional and the RMHD approximation is supported. The difference between K and K_P gradually becomes large gradually. The difference in run 1 is relatively large compared to that in run 2. We have to keep in mind the possibility that the pre-calculation in run 1 has worked to add 3D compressible perturbations[9] to the initial condition and led to early generation of toroidal flows. Though it is interesting to study whether the plasma obeys to 3D compressible perturbations or incompressible perturbations, it is a tough work and should be left for future work. After the linear growth, both runs 1 and 2 show two peaks of K. The saturation levels of run 2 are as large as twice of those in run 1, suggesting that the time evolution of the former is more violent than the latter. After the saturation of K, K_P becomes much smaller than K. Namely, the toroidal flow dominates the fluid motions for $t > 400\tau_A$. Though FIG.4 shows only for $t < 600\tau_A$, we have carried out run 1 till $t \simeq 1300\tau_A$ and verified that the kinetic energy decays monotonically after the saturation. Below, we concentrate on studying the dynamics in run 2 and try to find out qualitative views the full MHD effects.

Next we study the Fourier components of the pressure. Figure 5(a) is the time evolutions of the spatial power spectra of the pressure with low m and n wave numbers. We find that the $(m,n) = (2,1)$ mode grows exponentially first. The $(1,1)$ mode also grows exponentially and finally overcomes the $(2,1)$ modes. In the late stage of the evolutions $t > 450\tau_A$, the $(1,1)$ mode remains as the most dominant modes. In the points of views of the kinetic energy growth, the saturation time of the $(2,1)$ mode, $t \simeq 400\tau_A$, coincide with the first weak saturation of the kinetic energy K of run 2 in FIG.4, whereas the clearest saturation of K coincide with the saturation time of the $(1,1)$ mode. It implies that the kinetic energy saturates when the driving force, the pressure gradient, is lost.

Note that the $(m,n) = (1,1)$ mode has two stages of the exponential growth, before and after $t \simeq 370\tau_A$ in FIG.5(a). The evolutions of the Fourier modes around the time are magnified in FIG.5(b). The growth of $(1,1)$ after the time is still exponential but slower than that before the time. Since the growth rate of this mode in the earlier stage is almost the same with that of the $(2,1)$ mode, the $(1,1)$ mode is considered being a side band of the $(2,1)$ mode. However, the $(1,1)$ mode becomes the dominant mode after the saturation of the $(2,1)$ mode and begin to grow with different growth rate. A crucial point is that the $(3,2)$ mode grows simultaneously and the distance between the three rational surfaces, $\iota/2\pi = 1/2$, $2/3$ and $1/1$ are narrow. Furthermore, as is shown later, the $(2,1)$ and $(3,2)$ mode structures are overlapping to each other. Therefore, the situation is similar to the dangerous scenario suggested from the RMHD simulations.

In FIG.6(a) and (b), the Fourier modes resonant to $\iota/2\pi = 1/2$ and $2/3$ are shown respectively. These two rational surfaces are the most dangerous ones in the DNS under the stellarator symmetry, that is, for middle or high wave number Fourier modes. We find both in FIG.6(a) and (b) that the lowest modes grows first. The components of the lowest mode numbers have the largest growth rates at each rational surfaces because of the large viscosity and the higher modes grow later as the consequent of the nonlinear interactions.

In FIG.7, the mean profile of the pressure $\langle p \rangle$ at some typical times are shown. At $t = 450\tau_A$, the mean profile of the pressure is quite different from the initial one. The pressure increase as the function of ρ at $\rho < 0.3$. The adverse pressure gradient is stable in the system, being consistent with the saturation of $(2,1)$ mode. At $t = 600\tau_A$, the pressure deformation proceeds. At this stage of the evolution, the magnetic surfaces are destroyed (figure is omitted) but there are remains of the magnetic surfaces, preventing the plasma from loosing the stored pressure instantaneously.

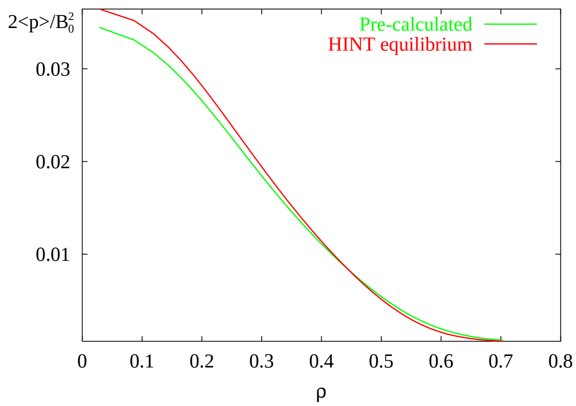

FIG. 3: Comparison of the initij:al pressure profile. The red line represents the ideal MHD equilibrium calculated by the HINT code. The green line represents the initial condition for run 1, provided by the pre-calculation under the stellarator symmetry. The vertical axis is normalized by $|\mathbf{B}|^2/2$ *of the HINT equilibrium.*

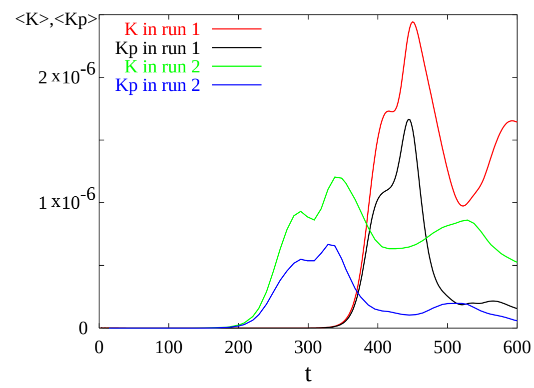

FIG. 4: Time evolution of the kinetic energy (green for run 1 and red for run 2) and poloidal contribution to it (blue and black for runs 1 and 2, respectively).

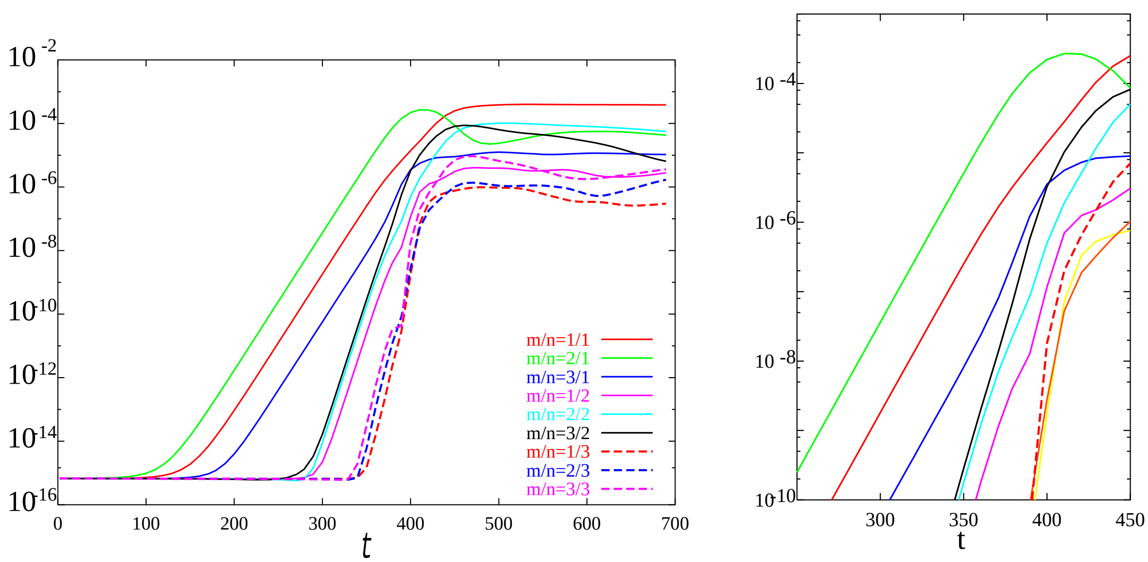

FIG. 5: Time evolutions of the Fourier power spectra of the pressure in Boozer coordinate.

3.2 Flow generation and pressure deformation

The growth of unstable modes shown above are observed in a poloidal section. In FIG.8, the color contours of the pressure on a vertically-elongated poloidal section are shown for $t = 350$, 400 and $600\tau_A$. The white lines represent streamlines drawn only by the poloidal velocity components. At $t = 350\tau_A$, the streamlines show formation of two anti-parallel vortex pairs associated with $(2,1)$ unstable modes. The two anti-parallel vortex pairs advect the pressure and mushroom-like pressure structures similar to those observed in run 1[10] are formed by the advection. At $t = 400\tau_A$, the

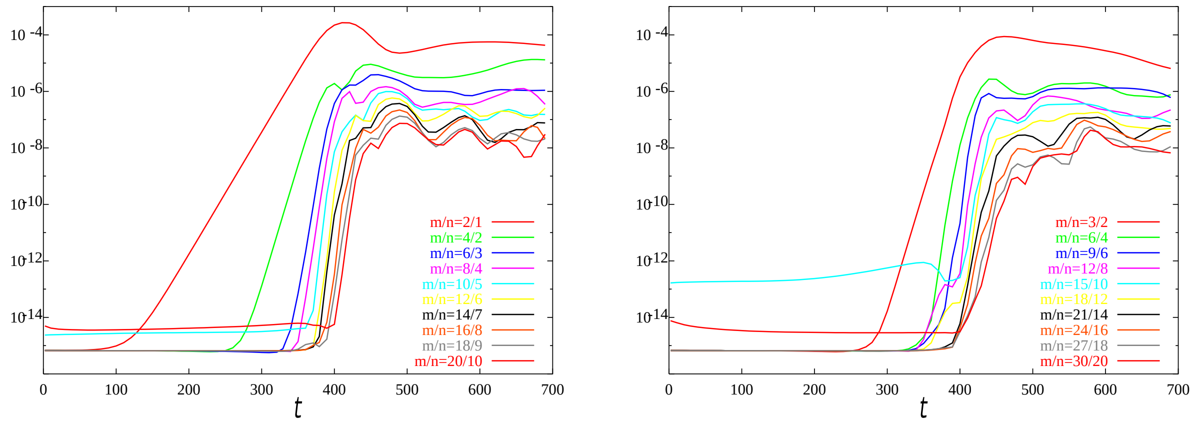

FIG. 6: Time evolutions of the spatial power spectra of the pressure associated with (a)$\iota/2\pi = 1/2$ and (b)$2/3$ rational surfaces. In (a), the lowest mode $m/n = 2/1$ and its higher harmonics up to $m/n = 20/10$ are shown. In (b), the lowest mode $m/n = 3/2$ and its higher harmonics up to $m/n = 30/20$ are shown.

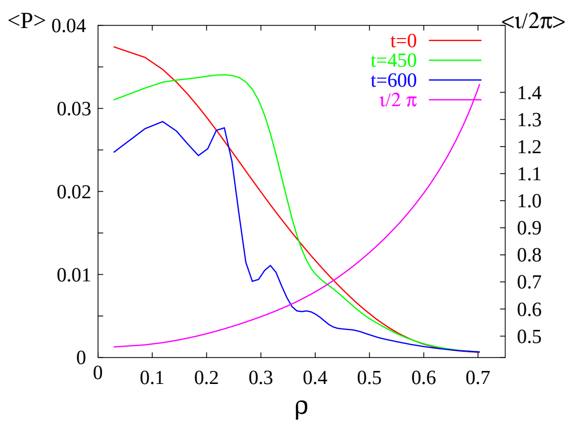

FIG. 7: The mean profile of the pressure at $t = 0$, 450 and $600\tau_A$. The vertical axis is normalized by $|\mathbf{B}|^2/2$ of the HINT equilibrium. The ι-profile of the initial equilibrium is shown simultaneously and tics of the $\iota/2\pi$ is shown in the right-hand-side of the bounding box.

streamlines show three vortex pairs. The emergence of the the third vortex pair is associated with excitations of $(m,n) = (3,2)$ modes seen in FIG.6(b). The third vortex pair is generated between the first two pairs, showing interactions of the $(3,2)$ and $(2,1)$ modes. At $t = 600\tau_A$, pressure deformation proceeds further. In these three figures, there are sinks or sources of the streamlines. They come from either the compressibility of fluid or from the toroidal contributions of the fluid motions. As far as we have verified by means of the visualization, generations of toroidal flows and occurrence of relatively large dilatation happens simultaneously at the same place.

In order to see the 3D properties of fluid motions, full-3D streamlines are drawn in FIG.9. Figures 9(a)-(c) are the 3D streamlines corresponds to FIG.8(a)-(c). In FIG.9(a)($t = 350\tau_A$), contributions of the toroidal flows to the vortices are not very large and the fluid motions look like quasi-two-dimensional. However, some streamlines are convergent and advected toward the toroidal direction forming spirals of streamlines. It suggests that compressibility and toroidal flows play finite roles in the flow topology. In FIG.9(b)($t = 400\tau_A$) it appears that the toroidal flow is as energetic as poloidal motions and in FIG.9(c) at $t = 600\tau_A$ the toroidal flows overcome the poloidal motions. Recall here that the toroidal motions have longer length scale than the poloidal motions with the same wave number. Thus toroidal motions are less dissipated by the viscosity compared to the poloidal motions. It implies that the toroidal motions are slow to decay once they are excited and influence long time behaviors. We also note that the dominance of the toroidal over poloidal flows may be strengthened because of the disruptive nature of this run, because the generation of the poloidal motions are stopped in these cases. In fact, the toroidal flows are much more dominant in run 2 than in run 1, as has been seen in FIG.4.

4 Concluding Remarks

The dynamics of the pressure driven modes in LHD is investigated by means of the two kinds of simulations, RMHD and DNS. The RMHD simulations are carried out aiming to investigate plasma stabilization mechanism. The stabilizing scenario proposed in Ref.[4] is confirmed in the higher β value than the previous work. The basic dynamics suggested by the RMHD simulations is that the plasma can be non-disruptive when the interaction of the modes with different helicities is weak while it can be disruptive when the interaction is strong. The DNS results also look similar to the RMHD results especially in the pressure deformation. Either non-disruptive or disruptive results are observed depending on the initial pressure profile in the DNS.

One of the remarkable results of the DNS runs is the appearance of the substantial toroidal flow. The flow generation may be associated with the pressure deformation, because the fraction of the toroidal flow in the kinetic energy is larger in the disruptive run than that in the non-disruptive run. The 3D compressible perturbation may also be related with the generation. Further investigation should be nesessary to understand how the substantial toroidal flow generation influences the stabilization mechanism scenario based on the RMHD results.

In summary, some basic views for the stabilization mechanism suggested by the RMHD results seem to be supported by DNS. The influences of the toroidal flows and the other full MHD effects on the mechanism will be carefully studied.

References

[1] MOTOJIMA, O., et al., Phys. Plasmas **6** (1999) 1843-1850.

[2] YAMADA, H., et al., Plasma Phys. Control. Fusion **43** (2001) A55-A71.

[3] SAKAKIBARA, S., et al., Nuclear Fusion **41** (2001) 1177-1183.

[4] ICHIGUCHI, K., et al., Nuclear Fusion **43** (2003) 1101-1109.

[5] MIURA, H., et al., Phys. Plasmas **8** (2001) 4870.

[6] HIRSHMAN, S.P., et al., Comp. Phys. Comm. **43** (1986) 143.

[7] LIANG, Y., et al., Plasma Phys. Control. Fusion **44** (2002) 1383.

[8] HARAFUJI, H., et al., J. Comp. Phys., **81** (1989) 169.

[9] NAKAJIMA, N., et al., to appear in J. Plasma Fusion and Res. SER. **6**.

[10] HAYASHI, T., et al., 19th IAEA Fusion Energy Conference, Lyon, 2002, IAEA-CN-94/TH/6-3.

[11] MIURA, H. and HAYASHI, T., to appear in J. Plasma Fusion and Res. SER. **6**.

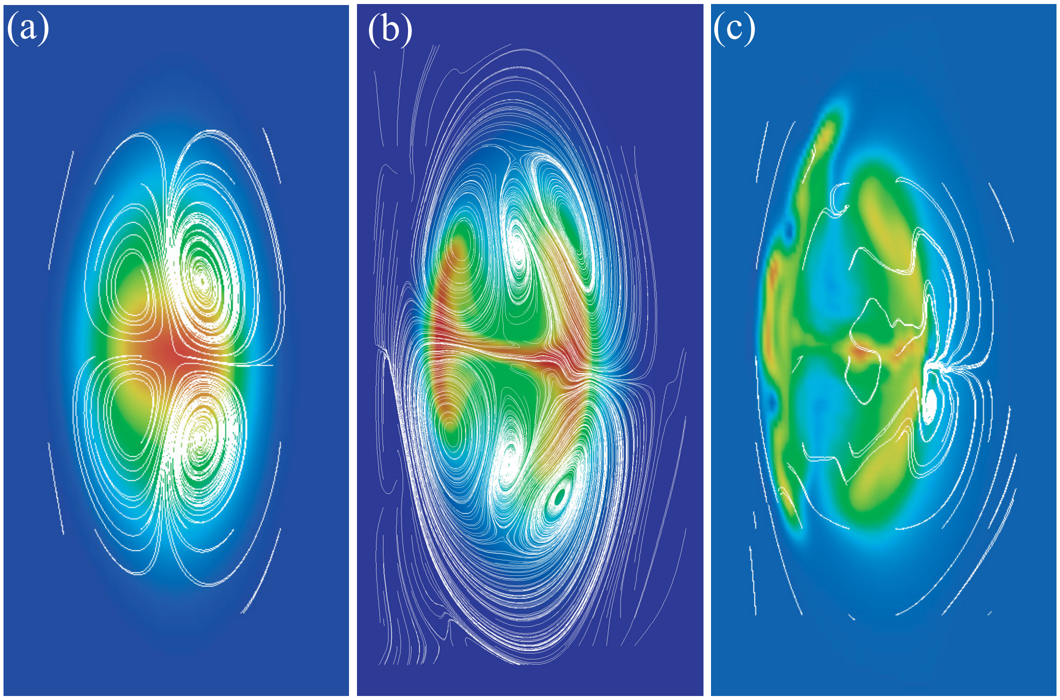

FIG. 8: Pressure contours and the two-dimensional streamlines on a vertically-elongated poloidal section at (a) $t = 350$*, (b)* 400 *and (c)* $600\tau_A$*. Sink or sources of the streamlines are attributed to toroidal motions or compressibility of the fluids.*

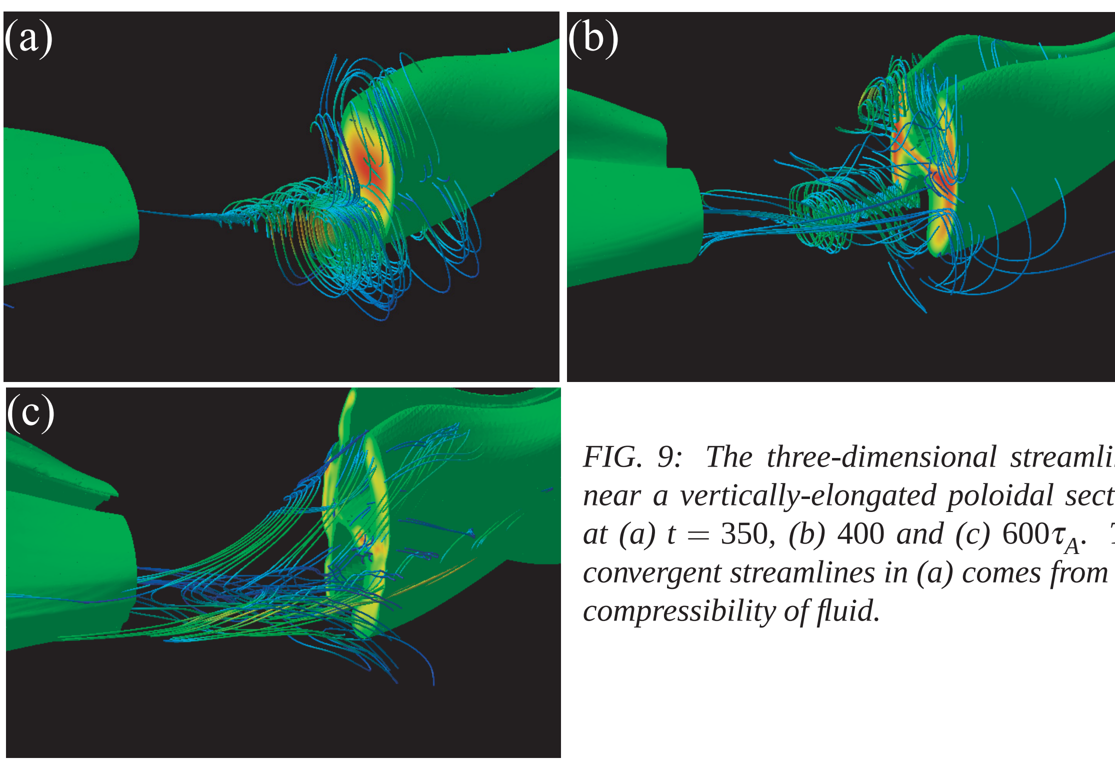

FIG. 9: The three-dimensional streamlines near a vertically-elongated poloidal section at (a) $t = 350$*, (b)* 400 *and (c)* $600\tau_A$*. The convergent streamlines in (a) comes from the compressibility of fluid.*